Composites Science and Technology 69 (2009) 612–619

Contents lists available at ScienceDirect

Composites Science and Technology

journal homepage: www.elsevier.com/locate/compscitech

Flow of non-Newtonian liquid polymers through deformed composites reinforcements

F. Loix [a], L. Orgéas [a,*], C. Geindreau [a], P. Badel [b], P. Boisse [b], J.-F. Bloch [c]

[a] CNRS – Universités de Grenoble, Laboratoire Sols-Solides-Structures-Risques, BP 53, 38041 Grenoble Cedex 9, France
[b] CNRS – INSA Lyon, Laboratoire de Mécanique des Contacts et des Structures, Bâtiment Jacquard, Rue Jean Capelle, F69621 Villeurbanne Cedex, France
[c] CNRS – Universités de Grenoble, Laboratoire de Génie des Procédés Papetiers, BP 65, 461 rue de la Papeterie, 38402 Saint-Martin d'Hères, Cedex 9, France

ARTICLE INFO

Article history:
Received 19 August 2008
Received in revised form 8 December 2008
Accepted 10 December 2008
Available online 24 December 2008

Keywords:
E. Liquid composites moulding (LCM)
B. Non-Newtonian liquid polymers
B. Permeability
C. Multiscale modeling
C. Computational analysis

ABSTRACT

The flow of non-Newtonian liquid polymers through fibrous reinforcements is a phenomenon which is often encountered during polymer composites manufacturing. In a previous work, we have proposed from a multiscale theoretical approach a method to model this phenomenon when the polymer can be regarded as a generalised Newtonian fluid [Orgéas et al. J. Non-Newtonian Fluid Mech. 2007; 145]. In this paper, the capability of the method is tested with power-law fluids flowing through deformed plain weave fabrics. For that purpose, the flow problem is firstly analysed at the mesoscale from numerical simulations performed on representative elementary volumes of the fabrics. The influences of both the current deformation of the fabrics and the fluid rheology on the macroscopic flow law are emphasised. Secondly, it is shown that the proposed method allows a nice fit of numerical results.

1. Introduction

Understanding, gauging and controlling physical phenomena occurring during the processing of fibre-reinforced polymer composites is crucial to produce optimised structural or functional components with such materials. Among these phenomena, (i) the evolution of fibrous microstructures as well as (ii) the flow of the liquid polymer through the fibrous reinforcements are still not very well understood and require a deeper analysis.

(i) Whatever the considered fibrous reinforcements, *i.e.* impregnated/dry short/long woven/non-woven networks of fibres/fibre bundles, the evolutions of their microstructures induced during the various stages of forming strongly affect their rheology [1–3]. This also significantly changes the possible flow of the liquid polymers through the fibrous networks [4–9].

(ii) The considered polymer matrixes, *i.e.* polymer blends, charged polymers or curing polymers, may exhibit complex rheologies, far from that of the idealised Newtonian fluid model. When non-Newtonian effects become pronounced, significant deviations from the flow of a standard Newtonian fluid through porous media are observed and cannot be neglected [10–15]. In such situations, the well-known Darcy's law is no longer relevant. Unfortunately, if the literature dealing with the flow of Newtonian fluid through fibrous media is abundant, much less is published concerning the flow of non-Newtonian fluids through anisotropic fibrous media, even in the very simple case where liquid polymers or polymer suspensions are assumed to behave, as a first rough but reasonable approximation, as purely non-linear viscous fluids. Consequently, resulting macroscopic models able to describe such macroscale flows are scarce [13,15–18].

In this work, we propose a method to model the second phenomenon at the macroscale, by investigating the impact of the evolution of the fibrous microstructures, *i.e.* the first phenomenon, on the macroscopic flow law. The method is based on a multiscale approach of which the theoretical background has been published in a previous work [18]. For that purpose, the flow problem at the fibre scale is first presented (Section 2). Theoretical results obtained from the upscaling process are briefly recalled (Section 3). A method to build continuous macroscopic flow laws is presented (Section 4). It is based on mesoscale simulations which are carried out on representative elementary volumes of fibrous microstructures. Its capability is here tested with generalised Newtonian fluids, *i.e.* power-law fluids, flowing through pre-sheared plain weaves (Section 5). In particular, the influences of both the current deformation of the plain weaves and the fluid rheology on the macroscopic flow law are emphasized.

* Corresponding author. Tel.: +33 4 76 82 70 73; fax: +33 4 76 82 70 43.
E-mail address: laurent.orgeas@hmg.inpg.fr (L. Orgéas).

0266-3538/$ - see front matter © 2008 Elsevier Ltd. All rights reserved.
doi:10.1016/j.compscitech.2008.12.007

2. Fluid flow problem at the mesoscale

We consider the slow and isothermal flow of an incompressible generalised Newtonian fluid through a rigid fibrous medium, by assuming a no slip condition at fluid–solid interfaces Γ. The fibrous medium, *e.g.* a textile reinforcement made up of continuous fibre bundles, is seen as an assembly of a large number of identical cells, called Representative Elementary Volume (REV), whose typical size l_{REV} is of the same order of magnitude as l_c, the characteristic thickness of sheared fluid at the heterogeneity scale (here the fibre bundle scale), *i.e.* $l_{REV} = \mathcal{O}(l_c)$. l_c is supposed to be very small compared to the size L_c upon which macroscopic pressure gradients occur. Hence, the scale separation parameter $\varepsilon = l_c/L_c$ is very small, *i.e.* $\varepsilon \ll 1$. Within the REV of volume Ω_{REV}, the flowing fluid occupies a volume Ω_f, whereas fibre bundles occupy a volume Ω_s. For the sake of simplicity, the flow within them is ignored in this study. The stress tensor $\boldsymbol{\sigma}$ of the considered flowing fluids is:

$$\boldsymbol{\sigma} = -p\boldsymbol{\delta} + \boldsymbol{\tau} \quad \text{with} \quad \boldsymbol{\tau} = 2\eta\mathbf{D}, \tag{1}$$

where p is the incompressibility pressure, $\boldsymbol{\delta}$ the identity tensor and where the extra stress $\boldsymbol{\tau}$ depends on both the shear viscosity η and the strain rate tensor $\mathbf{D} = (\nabla \otimes \mathbf{v} + \mathbf{v} \otimes \nabla)/2$, $\mathbf{v}$ being the local fluid velocity field. The shear viscosity η is assumed to be a function of the microscopic equivalent shear strain rate $\dot{\gamma}_{eq} = \sqrt{2\mathbf{D} : \mathbf{D}}$, *i.e.* $\eta(\dot{\gamma}_{eq})$. Many well-known rheological models belong to this fluid category: Newtonian fluids, power-law fluids, Cross fluids, Carreau–Yasuda fluids, regularised versions of Bingham or Herschel–Bulkley fluids... From the very simple Newtonian approximation, the other cited models constitute a first step to better account for the complex and non-Newtonian rheology of liquid polymers or polymer suspensions during the processing of polymer composites: they can capture the non-linear influence of strain rates on stress levels required to induce the flow of these complex fluids at finite strain or in steady state situations. Let us note that $\boldsymbol{\tau}$ can also be defined as the gradient of a volumetric viscous dissipation potential Φ:

$$\boldsymbol{\tau} = \frac{\partial \Phi}{\partial \mathbf{D}} = \frac{\partial \Phi}{\partial \dot{\gamma}_{eq}} \frac{\partial \dot{\gamma}_{eq}}{\partial \mathbf{D}} = \tau_{eq} \frac{\partial \dot{\gamma}_{eq}}{\partial \mathbf{D}} = 2\eta\mathbf{D}, \tag{2}$$

where the equivalent shear stress τ_{eq} is defined as:

$$\tau_{eq} = \frac{\partial \Phi}{\partial \dot{\gamma}_{eq}} = \eta\dot{\gamma}_{eq}, \tag{3}$$

so that the volumetric mechanical local dissipation $\mathscr{P}_{dis}$ is expressed as:

$$\mathscr{P}_{dis} = \boldsymbol{\tau} : \mathbf{D} = \tau_{eq}\dot{\gamma}_{eq}. \tag{4}$$

This study is restricted to fluids which verify $d\tau_{eq}/d\dot{\gamma}_{eq} > 0$. This assumption endows the so-defined dissipation potential Φ with the convexity property. It is required to ensure the solution unicity of the localisation problem (7) (see Section 3, [18]). For example, in case of power-law fluids, for which $\eta = \eta_0\dot{\gamma}_{eq}^{n-1}$ (η_0 being the positive consistency and n the power-law exponent), the last restriction imposes $n > 0$.

Finally, let us point out that when a homogeneous permeation experiment performed with a fibrous sample of length L_c is considered, the present fluid flow problem is driven by a balance between a macroscopic pressure gradient of characteristic value $\Delta p_c/L_c$ and viscous drag forces of characteristic value $f_c = \tau_c/l_c$, τ_c being the characteristic shear stresses induced by the local shearing of the fluid at a charateristic shear rate v_c/l_c [18]:

$$\frac{\Delta p_c}{L_c} = \mathcal{O}(f_c) = \mathcal{O}\left(\frac{1}{l_c}\tau_c\right) = \mathcal{O}\left(\frac{1}{l_c}\eta_c\frac{v_c}{l_c}\right) \quad \text{with } \eta_c = \eta\left(\frac{v_c}{l_c}\right). \tag{5}$$

3. Upscaling process: main results

The above local fluid flow problem was theoretically upscaled in previous studies for Newtonian fluids [19], power-law fluids [20,21], and more recently for generalised Newtonian fluids [18] by using the homogenisation method with multiple scale asymptotic expansions [22]. We briefly recall here the main results deduced from these studies.

3.1. Macroscopic balance equations

The homogenisation process shows that for generalised Newtonian fluids, the mass and momentum balance equations of the macroscopic equivalent continuum associated with the above local physics are, respectively [18]:

$$\begin{cases} \nabla \cdot \langle \mathbf{v} \rangle = 0, \\ \nabla \bar{p} = \mathbf{f}(\langle \mathbf{v} \rangle, \eta, \textit{microstructure}), \end{cases} \tag{6}$$

where $\nabla\bar{p}$ stands for the macroscopic pressure gradient, $\langle \mathbf{v} \rangle$ is the macroscopic velocity defined as the volume average of the first order component $\bar{\mathbf{v}}$ of the velocity field $\mathbf{v}$, and $\mathbf{f}$ is a macroscopic volumetric viscous drag force depending on $\langle \mathbf{v} \rangle$, the shear viscosity η and the fibrous microstructure.

3.2. First order localisation problem

In order to estimate the macroscopic flow law, *i.e.* the form of $\mathbf{f}$, the macroscopic velocity field $\langle \mathbf{v} \rangle$ must be determined. $\langle \mathbf{v} \rangle$ can be obtained by determining the first order periodic velocity field $\bar{\mathbf{v}}$ in a given REV, by solving the following localisation problem resulting from the homogenisation process [18]:

$$\begin{cases} \nabla \cdot \bar{\mathbf{v}} = 0 & \text{in } \Omega_f, \\ 2\nabla \cdot \left(\eta\left(\dot{\bar{\gamma}}_{eq}\right)\bar{\mathbf{D}}\right) = \nabla\bar{p} + \nabla\delta p & \text{in } \Omega_f, \\ \bar{\mathbf{v}} = \underline{0} & \text{on} \Gamma, \end{cases} \tag{7}$$

where the macroscopic pressure gradient $\nabla\bar{p}$ acts as a constant and given volume force in the whole REV, and δp is the first order periodic fluctuations of the pressure field around $\bar{p}$.

3.3. Properties and forms of the macroscopic flow law

When the flowing fluid is Newtonian, *i.e.* when $\eta = \eta_0$, it can be shown that the macroscopic flow law reduces to the well-known Darcy's law [23,19]:

$$\mathbf{f} = -\eta_0\mathbf{K}^{-1} \cdot \langle \mathbf{v} \rangle, \tag{8}$$

where $\mathbf{K}$ is the definite, positive and symmetric permeability tensor. When considering a power-law fluid, the linear Darcy's law (8) is not valid any more. However, it can further be proved that $\mathbf{f}$ is a homogeneous function of degree n of the average velocity $\langle \mathbf{v} \rangle$ [21]:

$$\mathbf{f}(\xi\langle \mathbf{v} \rangle) = \xi^n\mathbf{f}(\langle \mathbf{v} \rangle), \ \forall \xi \in \mathbb{R}^+. \tag{9}$$

For other generalised Newtonian fluids, relations (8) and (9) are no more satisfied. Nonetheless, it can be shown that the macroscopical drag force $\mathbf{f}$ is the gradient, with respect to $\langle \mathbf{v} \rangle$, of the volume averaged viscous dissipation $\langle \Phi \rangle$ [18]:

$$\mathbf{f} = -\frac{\partial\langle \Phi \rangle}{\partial\langle \mathbf{v} \rangle}. \tag{10}$$

As shown by (2), the viscous dissipation potential Φ can be expressed at microscopic scale as a function of $\dot{\gamma}_{eq}$. Similarly, the macroscopic dissipation potential $\langle \Phi \rangle$ can be expressed as a function of a macroscopic equivalent velocity v_{eq}, defined as a norm in the velocity space and depending on $\langle \mathbf{v} \rangle$:

$$\mathbf{f} = -\frac{\partial\langle\Phi\rangle}{\partial v_{eq}}\frac{\partial v_{eq}}{\partial\langle\mathbf{v}\rangle} = -f_{eq}\frac{\partial v_{eq}}{\partial\langle\mathbf{v}\rangle}, \tag{11}$$

where $f_{eq}(v_{eq})$ is the macroscopic equivalent drag force defined as

$$f_{eq} = \frac{\partial\langle\Phi\rangle}{\partial v_{eq}}. \tag{12}$$

Hence, the volume average mechanical dissipation $\langle\mathscr{P}_{dis}\rangle$ reads:

$$\langle\mathscr{P}_{dis}\rangle = \langle\boldsymbol{\tau}:\mathbf{D}\rangle = \langle\tau_{eq}\dot{\gamma}_{eq}\rangle = -\langle\mathbf{v}\rangle\cdot\mathbf{f} = f_{eq}v_{eq}. \tag{13}$$

By considering this latter equation and Eqs. (3), (4) and (12), it is important to notice that $\tau_{eq}(\dot{\gamma}_{eq})$ and $f_{eq}(v_{eq})$ play similar roles at the microscale and at the macroscale, respectively. Besides, (12), (13) show that when it is plotted in the velocity space, a macroscopic iso-dissipation (iso-$\langle\mathscr{P}_{dis}\rangle$) surface is an iso-$v_{eq}$ surface and also an iso-potential (iso-$\langle\Phi\rangle$) surface.

Consequently, the macroscopic flow law is entirely defined if relevant expressions of (i) $f_{eq}(v_{eq})$ and (ii) $v_{eq}(\langle\mathbf{v}\rangle)$ are proposed:

(i) As suggested in [9], the characteristic velocitic v_c involved in (5) can be linked with the equivalent velocity v_{eq} by using the following mass balance expression: $v_c = v_{eq}/\phi_c$, where ϕ_c may be expressed as the volume fraction of fluid effectively involved in the flow resistance. The analysis of the flow structure at mesoscale can give sense to this porosity. Indeed, by considering n_c, the number of fluid channels (cross-section l_c^2) mainly contributing to the flow in a given direction, S_{REV}, the REV area which is projected on a plane perpendicular to the given direction, a possible estimation of ϕ_c is:

$$\phi_c = n_c l_c^2/S_{REV}. \tag{14}$$

Please notice that n_c and l_c depend on the topology of the considered fibrous reinforcement, but they also depend on the topology of the fluid flow within it: they are estimated from the solution $\bar{\mathbf{v}}$ of the localisation problem (7) (see Section 4). Therefrom, the equivalent drag force f_{eq} can be expressed as a function of v_{eq} by accounting for physical arguments used to establish (5). In the case of a power-law fluid, this yields:

$$f_{eq} = \frac{\eta_0}{l_c}\left(\frac{v_{eq}}{\phi_c l_c}\right)^n. \tag{15}$$

(ii) In case of orthotropic macroscopic flow laws, whose orthotropy directions are noted $\mathbf{e}_{\mathrm{I}}$, $\mathbf{e}_{\mathrm{II}}$ and $\mathbf{e}_{\mathrm{III}}$, v_{eq} only depends on the velocity invariants V_{I},V_{II},V_{III} defined in (17). A frame-independent expression can be obtained by using the theory of representation of anisotropic tensor functions [18,24]. In case of a power-law fluid, this form is:

$$\mathbf{f} = -\frac{\eta_0}{l_c}\left(\frac{v_{eq}}{\phi_c l_c}\right)^n\left(\frac{1}{V_{\mathrm{I}}}\frac{\partial v_{eq}}{\partial V_{\mathrm{I}}}\mathbf{M}_{\mathrm{I}} + \frac{1}{V_{\mathrm{II}}}\frac{\partial v_{eq}}{\partial V_{\mathrm{II}}}\mathbf{M}_{\mathrm{II}} + \frac{1}{V_{\mathrm{III}}}\frac{\partial v_{eq}}{\partial V_{\mathrm{III}}}\mathbf{M}_{\mathrm{III}}\right)\cdot\langle\mathbf{v}\rangle \tag{16}$$

where the microsctructure tensors $\mathbf{M}_i$ and the velocity invariants V_i are, respectively, defined as (i = I, II, III, no summation on the indices i):

$$\mathbf{M}_i = \mathbf{e}_i\otimes\mathbf{e}_i \quad\text{and}\quad V_i = \sqrt{\langle\mathbf{v}\rangle\cdot\mathbf{M}_i\cdot\langle\mathbf{v}\rangle}. \tag{17}$$

For example, when the orthotropy reference frame ($\mathbf{e}_{\mathrm{I}},\mathbf{e}_{\mathrm{II}},\mathbf{e}_{\mathrm{III}}$) corresponds to the current reference frame ($\mathbf{e}_1,\mathbf{e}_2,\mathbf{e}_3$), the V_i's correspond to $|\langle v_i\rangle|$. Various convex forms of $v_{eq}(V_i)$ may be proposed. That proposed in [18] is expressed as:

$$v_{eq}^m = v_{eqa}^m + v_{eqb}^m \tag{18}$$

with

$$v_{eqa}^{m_a} = V_{\mathrm{I}}^{m_a} + \left(\frac{V_{\mathrm{II}}}{A}\right)^{m_a}, \quad v_{eqb} = \frac{V_{\mathrm{III}}}{B} \quad\text{and}\quad m = \frac{m_b V_{\mathrm{I}}^2 + m_c V_{\mathrm{II}}^2}{V_I^2 + V_{\mathrm{II}}^2}. \tag{19}$$

Hence, $v_{eq} = V_{\mathrm{I}}$ when the macroscopic flow is parallel with the orthtropy direction $\mathbf{e}_{\mathrm{I}}$. Likewise, as shown in Fig. 5d, the constitutive parameters A and B characterise the anisotropy of iso-v_{eq} surfaces along the principal axes $\mathbf{e}_{\mathrm{II}}$ and $\mathbf{e}_{\mathrm{III}}$. Lastly, the constitutive parameters m_i's control the curvatures of these surfaces [18]. They equal *2* for Newtonian fluids so that (16) reduces to the Darcy's law (8).

4. Method to build the macroscopic flow law

To summarise, from the knowledge of the shear viscosity η of the flowing fluid, the orthotropic macroscopic flow law (16)–(19) only requires seven additional constitutive parameters: l_c,n_c,A,B,-m_a,m_b and m_c, ϕ_c being a function of l_c and n_c (see (14)). The general procedure to determine them consists in:

(i) *Finding the symmetries of the flow* - as shown for example in [14], problem (7) is solved for a set of pressure gradients $\nabla\bar{p}$ with identical norm and various orientations in order to look for symmetries. The resulting pairs ($\mathbf{f}$,$\langle\mathbf{v}\rangle$) are recorded. If the flow law exhibits three orthogonal symmetry planes, this allows to determine the microstructures vectors $\mathbf{e}_{\mathrm{I}}$, $\mathbf{e}_{\mathrm{II}}$ and $\mathbf{e}_{\mathrm{III}}$ and corresponding microstructure tensors $\mathbf{M}_{\mathrm{I}}$, $\mathbf{M}_{\mathrm{II}}$ and $\mathbf{M}_{\mathrm{III}}$.

(ii) *Analysing the flow along* $\mathbf{e}_I$ *direction* - as proposed in [9], a micro-scale analysis of the flow problem (7) is performed in order to estimate n_c. From the knowledge of S_{REV}, this allows expressing ϕ_c as a function of l_c only (see (14)). Then, l_c is determined from the macroscopic flow law (16)–(19), which in this particular situation is expressed as:

$$\mathbf{f} = -\frac{\eta_0}{\phi_c l_c^2}\left(\frac{|\langle v_{\mathrm{I}}\rangle|}{\phi_c l_c}\right)^{n-1}\langle v_{\mathrm{I}}\rangle\mathbf{e}_{\mathrm{I}} \tag{20}$$

(iii) *Analysing the flow along* $\mathbf{e}_{II}$ *and* $\mathbf{e}_{III}$ *directions* - in these two situations, the macroscopic flow law (16)–(19), respectively, reduces to:

$$\mathbf{f} = \frac{-\eta_0}{\phi_c A^2 l_c^2}\left(\frac{|\langle v_{\mathrm{II}}\rangle|}{\phi_c A l_c}\right)^{n-1}\langle v_{\mathrm{II}}\rangle\mathbf{e}_{\mathrm{II}} \quad\text{and}$$
$$\mathbf{f} = \frac{-\eta_0}{\phi_c B^2 l_c^2}\left(\frac{|\langle v_{\mathrm{III}}\rangle|}{\phi_c B l_c}\right)^{n-1}\langle v_{\mathrm{III}}\rangle\mathbf{e}_{\mathrm{III}} \tag{21}$$

From these two relations, the constitutive parameters A and B can be easily determined.

(iv) *Building iso-dissipation surfaces* - the method is similar to step (i). However, the norms of the pressure gradients $\nabla\bar{p}$ must be adjusted so that each pair ($\mathbf{f}$,$\langle\mathbf{v}\rangle$) dissipates the same mechanical power $\langle\mathscr{P}_{dis}\rangle_0$. When fluid viscosity is governed by a power-law, this can be easily done from numerical simulations performed in step (i) by considering the homogeneity property (9) and the mean power given in (13) [15]. Indeed, a known flow pair ($\mathbf{f}_a$,$\langle\mathbf{v}\rangle_a$) dissipating $\langle\mathscr{P}_{dis}\rangle_a$ can then be used in order to calculate a flow pair ($\langle\mathbf{v}\rangle_0$, $\mathbf{f}_0$) dissipating a given $\langle\mathscr{P}_{dis}\rangle_0$:

$$\langle\mathbf{v}\rangle_0 = \xi\langle\mathbf{v}\rangle_a \quad\text{and}\quad \mathbf{f}_0 = \xi^n\mathbf{f}_a \quad\text{with}\quad \xi = \left(\frac{\langle\mathscr{P}_{dis}\rangle_0}{\langle\mathscr{P}_{dis}\rangle_a}\right)^{\frac{1}{n+1}}. \tag{22}$$

For other generalised Newtonian fluids, this rule can not be applied and a simple iterative algorithm can, for example, be implemented to gradually adapt the pressure gradient

norm in order to generate a flow dissipating the targeted mechanical mean power $\langle \mathscr{P}_{dis} \rangle_0$. In those cases, problem (7) has to be solved for each tested pressure gradient.

(v) *Fitting the form (18), (19) of v_{eq} to numerical iso-dissipation surfaces obtained in step (iv)* - this allows obtaining the three remaining constitutive parameters m_a,m_b and m_c.

5. Application to deformed textile reinforcements

The methodology described in the previous section is here applied to model the flow of a power-law fluid through woven fabrics. These types of flows may be typically encountered in the RTM process or during the sheet forming of fibre-reinforced polymer composite sheets. In this example, the RTM process is adressed: the roles of both the shear pre-deformation of the dry textile and the fluid rheology are emphasized.

5.1. Mesostructure

We consider a plain weave with identical warp and weft fibre bundles. The non-deformed shape is defined by means of circle arcs whose dimensions are given in Fig. 1. The analysis of the shear pre-deformation of the plain weave was extensively studied in [2]. Its relevance has been recently demonstrated in [25]. Briefly, by accounting for the periodicity of the considered textile, Finite Element (FE) simulations were carried out on solid REV's of the plain weave (see Fig. 2a and c). Such simulations were performed accounting for (i) large transformations, (ii) bundle–bundle contacts and (iii) the transverse isotropy of fibre bundles, assumed to behave like hypoelastic bodies. The reader is referred to [2,25] for details about this analysis. As an example, Fig. 2c illustrates the deformed shape of the solid REV of the plain weave shown in Fig. 2a after an in-plane shear pre-deformation of 53°, *i.e.* far beyond the locking angle. From the as-deformed solid REV's, associated fluid REV's (see Fig. 2b and d) were built, in order to solve the localisation problem (7). The method used to build fluid REV's from the solid REV's is described in [9].

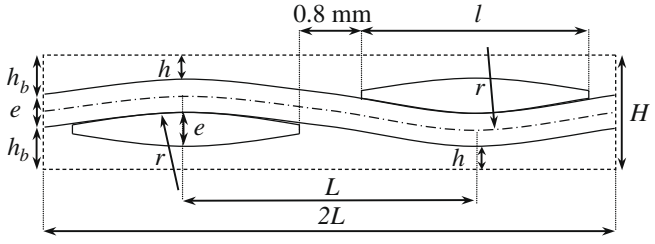

Fig. 1. Cross-section of the considered plain weave and its corresponding dimensions in the non-deformed configuration. Curvature radius $r = 9.82$ mm, fibre bundle width $l = 3.2$ mm, length of the fluid REV $2L = 8$ mm, fibre bundle thickness $e = 0.37$ mm, air-gap between layers $2h$, air-gap on the lateral boundaries $2h_b$ and fluid REV thickness H. When $h = 0$ mm, then $h_b \approx 0.18$ mm and $H \approx 0.74$ mm. The dashed lines represent the periodic boundaries of the fluid REV.

5.2. Numerical results and fit of the macroscopic flow law

For convenience, the reference frame ($\mathbf{e}_1$,$\mathbf{e}_2$, $\mathbf{e}_3$) has been here aligned with the directions of the rhombus-REV diagonals and the REV thickness (see Fig. 2b and d). Therefrom, a set of unit macroscopic pressure gradients $\nabla\bar{p}$ with various orientation angles θ, φ (see Fig. 2b) has been imposed to the fluid REV's in order to compute the velocity fields $\langle \mathbf{v} \rangle$ (step (i) of Section 4). For each pressure gradient, the localisation problem (7) has been solved with a mixed pressure–velocity formulation of the FE method implemented in Comsol Multiphysics [9,14,15,18].

Results showed that for the considered power-law fluids and for the considered sheared configurations of the plain weave the macroscopic flow law always displays at least three orthogonal symmetry planes, whose normal corresponds to $\mathbf{e}_1$, $\mathbf{e}_2$ and $\mathbf{e}_3$. Hence, even if the considered non-deformed and deformed textiles do not exhibit orthotropy and have a higher degree of anisotropy, the macroscopic flow law displays orthotropy. Consequently, this allows us using the orthotropic flow law ((16)–(19)) and to work with the velocity invariants V_i's.

Then, flows along the $\mathbf{e}_i$ directions were analysed (step (ii) and (iii) of Section 4) in order to dertemine n_c, l_c, A and B. As in [9], the number of fluid channels along the $\mathbf{e}_1$ direction n_c was estimated to

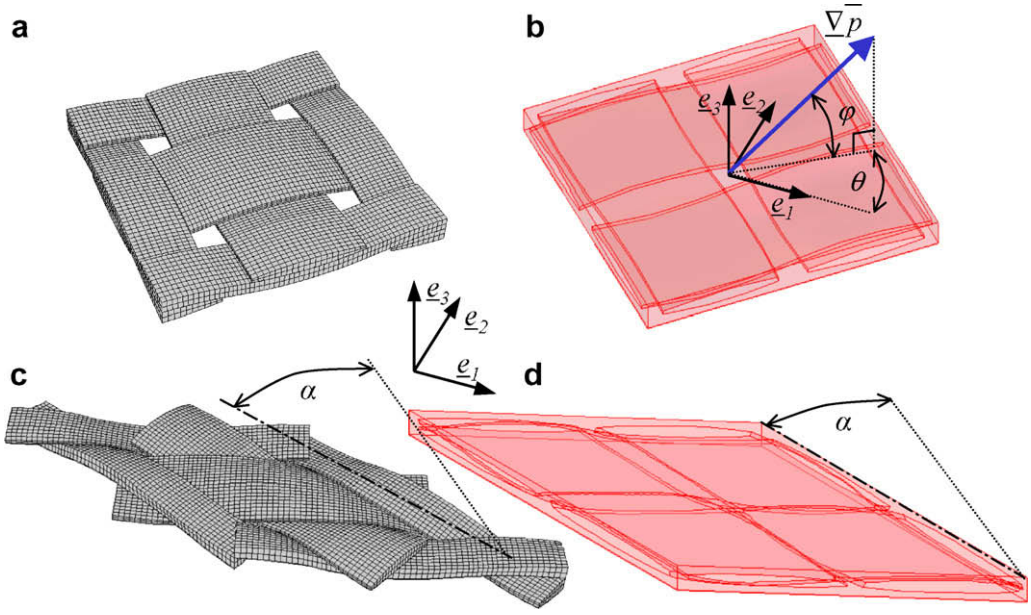

Fig. 2. Solid and fluid REV's for the non-deformed configuration (a,b) and after a shear deformation with angle α of 53° (c, and d). Reprensentation of $\underline{\nabla}\bar{p}$ as a function of the orientation angles θ and φ.

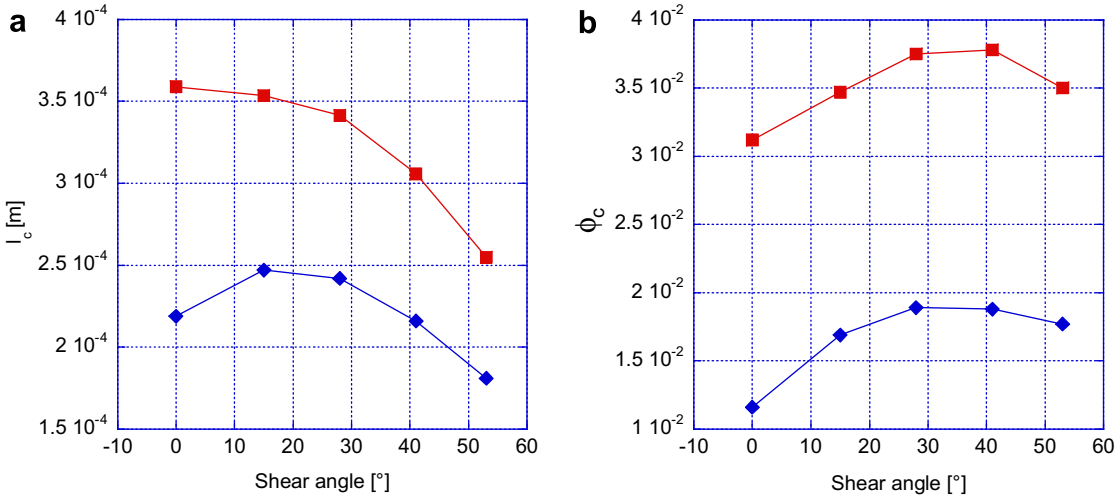

Fig. 3. Characteristic length l_c (a) and active porosity ϕ (b) involved in (18) and (19) for different shear angles of the woven fabric, for a Newtonian fluid (■) and for a power-law fluid with $n = 0.3$ (♦).

2. The evolutions of l_c and ϕ_c, and those of A and B have been reported as functions of the shear angle α in the graphs of Figs. 3a and b) and 4a and b), respectively.

Therefrom, the computed pairs $(\mathbf{f}, \langle \mathbf{v} \rangle)$ have been adjusted with (22) in order to dissipate a same given mechanical power $\langle \mathscr{P}_{dis} \rangle = 100\,\mathrm{Wm}^{-3}$ (step (iv) of Section 4). Results are illustrated by the stars plotted in the four graphs of Fig. 5, which represent numerical iso-dissipative points obtained for four different configurations, namely the non-sheared (a,b) and the 53°-sheared (c,d) configurations, and for different fluids, namely a Newtonian fluid with $\eta_0 = 1$Pa s (a,c) and a power-law fluid with $\eta_0 = 1$Pa s^n and $n = 0.3$ (b,d).

Lastly, the continuous surface (18), (19) was fitted to the obtained iso-dissipative numerical points, in order to estimate the m_i's (step (v) of Section 4). This was achieved with Matlab by following the Nelder–Mead algorithm used for multidimensional unconstrained non-linear minimization. Satisfying results have been reached in the sense that the mean relative error per numerical point is less than 5%, whatever the studied deformed configurations and the considered fluids. Corresponding fitted surfaces are plotted in Fig. 5. The evolutions of the as-determined m_i's with the shear angle are reported in Fig. 6.

5.3. Discussion

Whatever the considered (non)-deformed fibrous reinforcement and considered fluid rheology (*i.e.* generalised Newtonian fluids), results shown in Figs. 3, 5, 4, 6 together with those already obtained in [18] first prove that the proposed method allows obtaining a fairly relevant macroscopic flow law. In particular, the continuous expression (18), (19) proposed for v_{eq} gives a nice fit of numerical iso-dissipative points, as shown in Fig. 5.

Besides, these results also underline the strong and complex coupling between the REV microstructure and the flowing fluid rheology. More precisely, they bring up a first set of comments that are valid both for Newtonian and power-law fluids:

- As already pointed out in previous studies dedicated to Newtonian fluids [4–9], shearing the woven fabric induces noticeable changes of the macroscopic flow law. This is also the case for power-law fluids. As shown in Figs. 3 and 4, constitutive parameters l_c, ϕ_c, A and B display complex evolutions with the shearing angle, and these evolutions are qualitatively similar for Newtonian and power-law fluids. Notice that these changes can also be gauged from iso-dissipation surfaces plotted in Fig. 5. Indeed, for the same dissipated power, iso-dissipation surfaces are

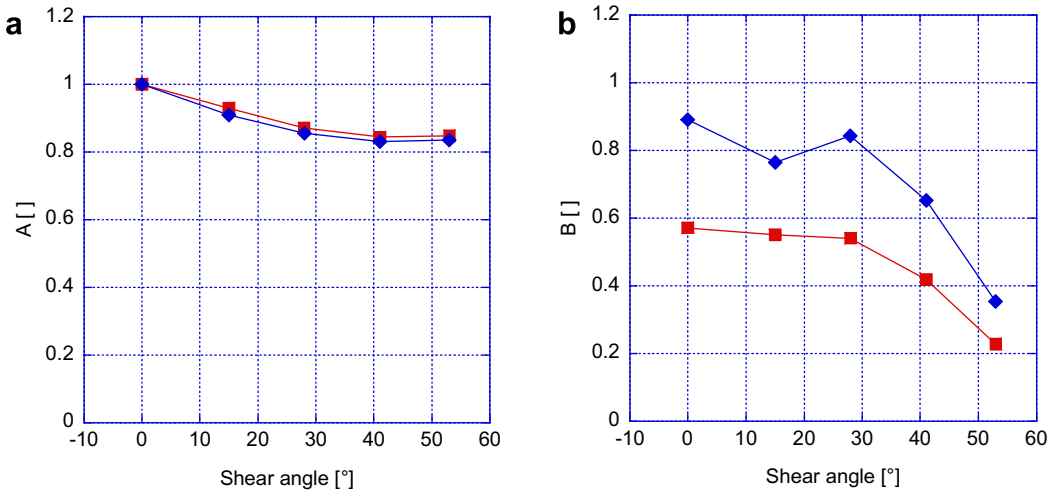

Fig. 4. Parameters $A = \langle v_{\mathrm{II}} \rangle / \langle v_{\mathrm{I}} \rangle$ (a) $B = \langle v_{\mathrm{III}} \rangle / \langle v_{\mathrm{I}} \rangle$ (b) involved in (18), (19) for different shear angles of the woven fabric, for a Newtonian fluid (■) and for a power-law fluid with $n = 0.3$ (♦).

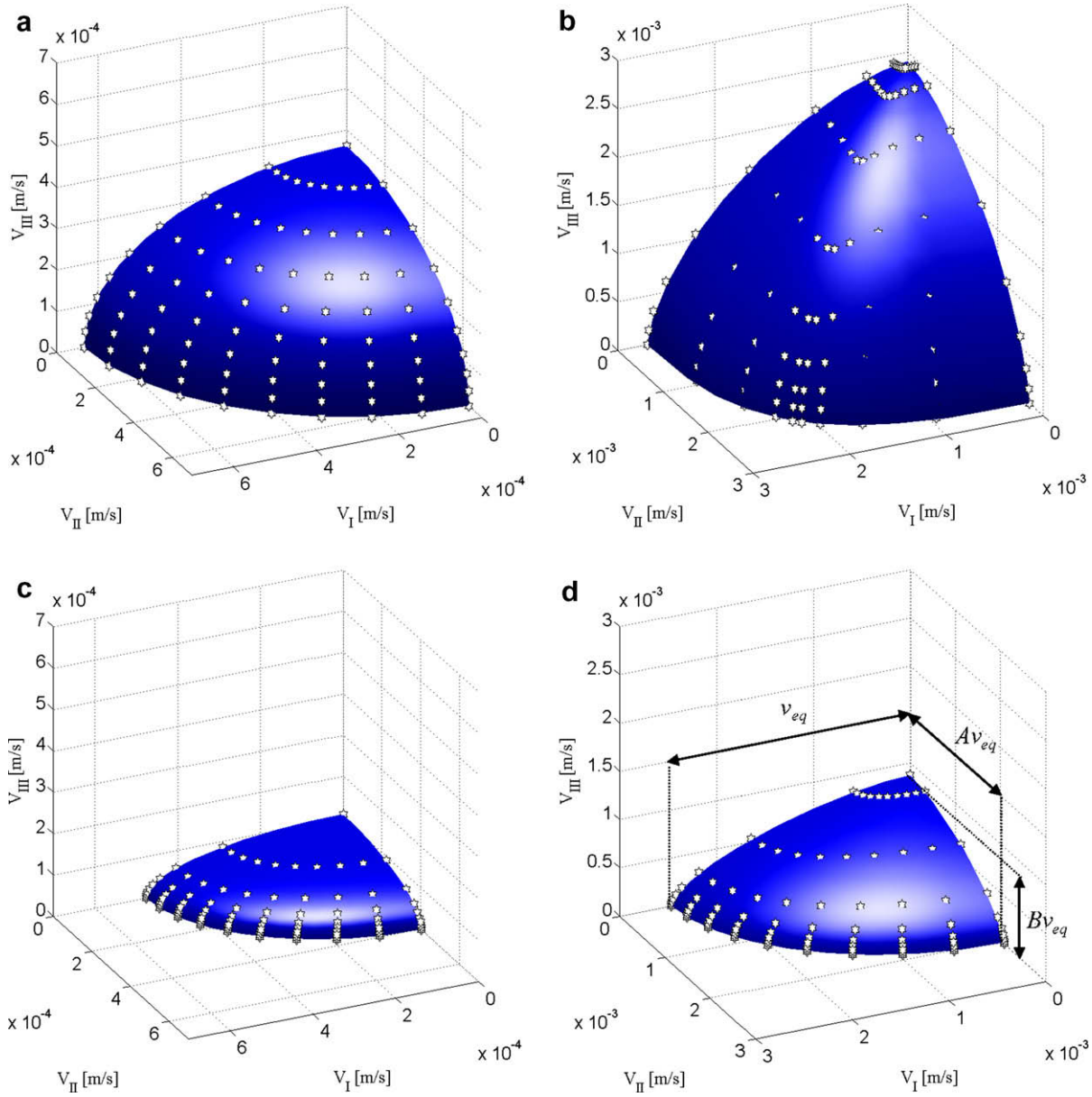

Fig. 5. Iso-dissipation surfaces (100 W/m^3) in the equivalent velocity (v_{eq}) space for the non-deformed (a and b) and 53°-sheared (c and d) configurations. On the left graphs (a and c) a Newtonian fluid ($n = 1$) is considered. On the left graphs (b and d) a power-law fluid with shear thinning rheology ($n = 0.3$) is considered. Numerical results (stars) have been determined by solving the localisation problem (7) while the continuous surface is modelled by phenomenological Eqs. (18), (19). The parameters of the continuous surfaces are depicted on Figs. 3, 4 and 6.

approximately twice as small after a shearing angle of 53^o, showing that the flow is much more difficult in this case than for the non-deformed case.

- Fig. 4 shows that (i) A and B are lower than 1 and (ii) a decrease of A and B as α increases. This reveals that (i) the in-axis flow becomes easier and easier as the flow direction goes from $\mathbf{e}_{\mathrm{III}}$, $\mathbf{e}_{\mathrm{II}}$ and $\mathbf{e}_{\mathrm{I}}$, respectively, and (ii) the intensity of the flow anisotropy is increased with the shearing angle: for example, iso-dissipation surfaces sketched in Fig. 5 are more stretched when $\alpha = 53^o$ than when $\alpha = 0^o$.

Likewise, current results also emphasise noticeable differences between Newtonian and shear thinning power-law flows:

- The characteristic porosity ϕ_c and thickness of sheared fluid l_c are smaller for the shear thinning power-law fluid. The trend observed for ϕ_c is entirely due to that observed for l_c, as suggested by (14): indeed, S_{REV} is a purely geometrical parameter and n_c has here been found identical for Newtonian and power-law fluids. The decrease of l_c with the power-law exponent n when $0 < n \leqslant 1$ is in turn something which is usually admitted for shear thinning fluids. It is directly correlated with the concentration of local shear stresses (and hence shear strain rates) near fluid–solid interfaces Γ as $n \to 0$.
- Fig. 5 shows that whatever the shear angle and for the considered flow regimes, *i.e.* for which the intrinsic volume average of the local shear rate $\dot{\gamma}_{eq}$ is above 1 s^{-1}, shear thinning flows are easier to achieve than Newtonian ones. Indeed, for the same and given dissipated mechanical power, velocities are approximately five to ten times as high for the shear thinning fluid. In other words, by accounting for (6) and (20), pressure gradients $\mathbf{V}\bar{p} = -2.4 \times 10^{-1}\mathbf{e}_{\mathrm{I}}$ and $\mathbf{V}\bar{p} = -10^{-2}\mathbf{e}_{\mathrm{I}}$ [MPa m^{-1}] are required to induce a velocity $\langle \mathbf{v} \rangle = 10^{-3}\mathbf{e}_{\mathrm{I}}$ [m s^{-1}] for the Newtonian and power-law fluids, respectively.

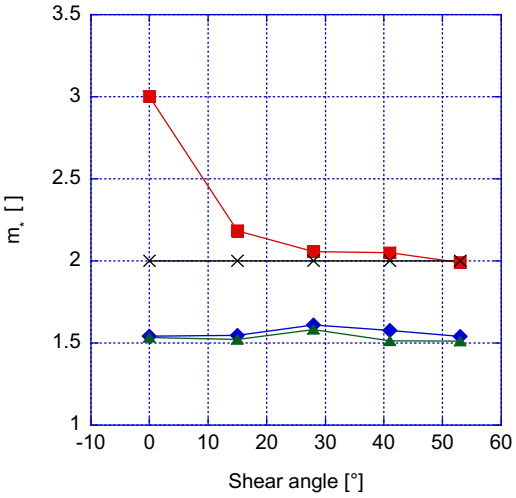

Fig. 6. Parameters m_a (■), m_b (♦) and m_c (▲) involved in (18), (19) for different shear angles of the woven fabric, for a Newtonian fluid and for a power-law fluid with $n = 0.3$. These parameters are all equal to 2 for a newtonian fluid (×). They have been used to plot continuous surfaces depicted in Fig. 5.

- For the non-deformed plain weave, the macroscopic flow law exhibits isotropy in the $(\mathbf{e}_\mathrm{I},\mathbf{e}_\mathrm{II})$ plane, since the in-axis flows have the same intensity ($A = 1$, see Fig. 4) and the curvature of the iso-dissipation surface is constant ($m_a = 2$, see Fig. 6). This is due to the particular geometry of the plane weave in this configuration (which is such that $\langle\mathbf{v}\rangle = a\mathbf{e}_\mathrm{I}$ when $\mathbf{V}\bar{p} = \mathbf{e}_\mathrm{I}$ and $\langle\mathbf{v}\rangle = a\mathbf{e}_\mathrm{II}$ when $\mathbf{V}\bar{p} = \mathbf{e}_\mathrm{II}$) and to the linearity of the macroscopic flow law (8). Even if the in-axis flows still have the same intensity ($A = 1$, see Fig. 4), such a planar isotropy is however broken for the shear thinning fluid since the curvature of its iso-dissipation surface varies ($m_a \approx 3$, see Fig. 6): the macroscopic flow law here exhibits tetratropy in the $(\mathbf{e}_\mathrm{I},\mathbf{e}_\mathrm{II})$ plane. A similar loss of symmetry has already been emphasized previously when studying the transverse flow of power-law fluids though square arrays of parallel fibres with circular cross-sections [14]. Its impact on the fluid flow is for instance illustrated in Fig. 7, where the directions of two imposed pressure gradients ($\varphi = 0°$, $\theta = 10°$ and $\theta = 45°$) and of their two associated velocities are depicted relatively to the iso-v_{eq} surface for the Newtonian flow (a) and for the shear thinning flow (b). In each case, the pressure gradient direction (dashed line) is perpendicular to the iso-dissipation surface, in accordance with the normality rule deduced from (11). Likewise, in the Newtonian case, due to the in-plane isotropy, the velocity (continuous line) is always aligned with the imposed pressure gradient (Fig. 7a). This is still the case for the power-law fluid when $\theta = 45°$ (see Fig. 7b), $\theta = 0°$ (see (20)) and $\theta = 90°$ (see (21)a), since these directions belongs to the symmetry planes of the flow law. Elsewhere, *i.e.* for other values of θ, this is no more valid. For example, as sketched in Fig. 7b, a noticeable deviation of an angle $\lambda \approx 13°$ is observed between the imposed pressure gradient and the resulting velocity when $\theta = 10°$.
- Possible measures of the intensity of the orthotropy can be extracted from (20), (21) by forming the following ratios: $|\langle v_\mathrm{II}\rangle(\mathbf{V}\bar{p} = \mathbf{e}_\mathrm{II})| / |\langle v_\mathrm{I}\rangle(\mathbf{V}\bar{p} = \mathbf{e}_\mathrm{I})| = A^{(n+1)/n}$ and $|\langle v_\mathrm{III}\rangle(\mathbf{V}\bar{p} = \mathbf{e}_\mathrm{III})| / |\langle v_\mathrm{I}\rangle(\mathbf{V}\bar{p} = \mathbf{e}_\mathrm{I})| = B^{(n+1)/n}$. The more these ratios differ from 1, the higher the orthotropy intensity. For the non-deformed plain weave, they are, respectively, equal to 1 and to 0.32 for the Newtonian fluid, whereas they are equal to 1 and to 0.63 for the power-law fluid: the orthotropy intensity is much more pronounced for the Newtonian fluid for this situation. This trend is completely reversed and amplified when the shear angle equal 53°. Indeed, the above ratios are then equal to 0.72 and to 0.05 for the Newtonian fluid, whereas they are equal to 0.49 and to 0.01 for the power-law fluid.

6. Conclusions

The flow of non-Newtonian viscous polymers through textile reinforcements is often encountered during polymer composites processing. To better understand this phenomenon, flows of Newtonian and power-law fluids through sheared plain weaves were studied from mescocale numerical simulations. These simulations were performed by using realistic REV's of the considered textiles [2,25], and by following guidelines provided the homogenisation method with multiple scale asymptotic expansions [21,18].

Whatever the flowing fluid, the major role of the shear deformation of the textile reinforcement was emphasised: shearing the plain weave leads to noticeable increase of the resistance as well as the anisotropy of the macroscopic fluid flow. This should be

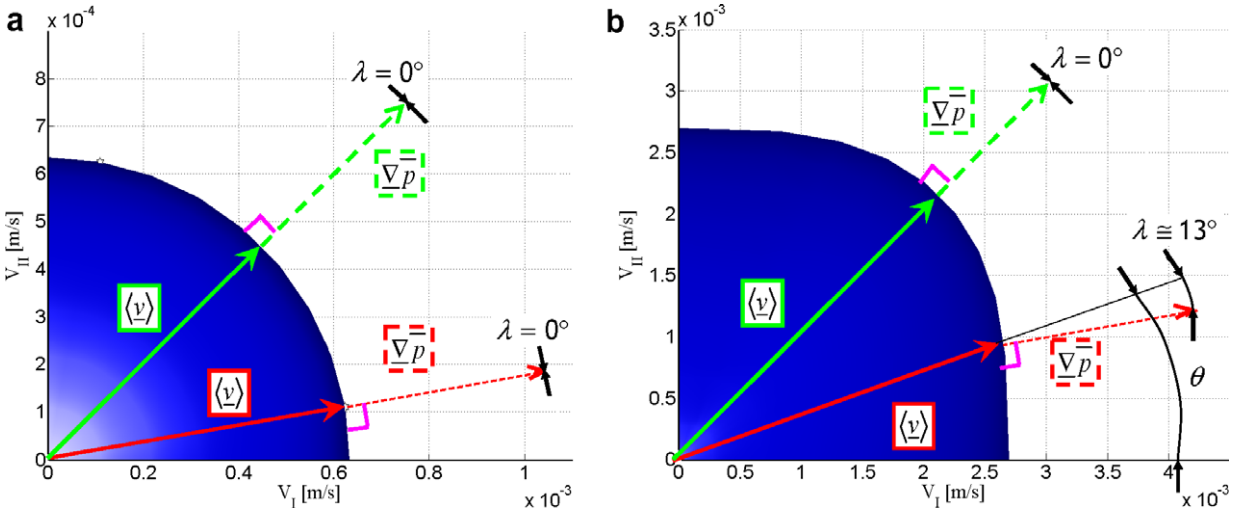

Fig. 7. View in the $(V_\mathrm{I}, V_\mathrm{II})$ plane of iso-dissipation surfaces (100 W/m^3) in the non-deformed configuration for a Newtonian fluid (a) and for a power-law fluid ($n = 0.3$) (b). Two differently oriented pressure gradients (red and green) are imposed with $\varphi = 0°$, $\theta = 10°$ and $\theta = 45°$ (dashed lines). Resulting velocities are depicted in continuous line. (For interpretation of the references in color in this figure legend, the reader is referred to the web version of this article.)

taken into account in macroscale simulations of polymer composites processing.

Besides, major differences were underlined depending on the flowing fluid. As expected, the shear thinning power-law fluid offers much less resistance than the Newtonian one, at high local shear strain rates and for the same consistency. Moreover, it has been shown that the anisotropy magnitude strongly depends on the flowing fluid and is highly linked with the pre-shearing of the fibrous network. Lastly, it was found that the macroscopic flow of the shear thinning fluid could exhibit a higher degree of anisotropy. The two last differences can induce noticeable changes on the orientation of the macroscopic flow. These effects should also be taken into account in macroscale simulations of polymer composites processing.

To do so, we have proposed a method to build the macroscopic flow law for generalised Newtonian fluids through porous media [18]. This method is based on the determination and the modelling of iso-dissipation surfaces. In this work, its relevance was emphasised in case of power-law fluids flowing through deformed textiles, by using mesoscale simulations. It must be pointed out that iso-dissipation surfaces could also be built from experimental data. It is also important to notice that the proposed macroscopic permeation law could be implemented without major difficulties in mold filling simulation software.

References

[1] Buet-Gautier K, Boisse P. Experimental analysis and modeling of biaxial mechanical behavior of woven composite reinforcements. Exp Mech 2001;41:260–9.

[2] Badel P, Vidal-Sallé E, Boisse P. Computational determination of in-plane shear mechanical behaviour of textile composite reinforcements. Comput Mater Sci 2007;40:439–48.

[3] Dumont P, Vassal J-P, Orgéas L, Michaud V, Favier D, Manson JAE, et al. Processing, characterisation and rheology of transparent concentrated fibre bundle suspensions. Rheol Acta 2007;46:639–51.

[4] Hammami A, Trochu F, Gauvin R, Wirth S. Directional permeability measurement of deformed reinforcement. J Reinf Plast Compos 1996;15:55262.

[5] Lai CL, Young WB. Model resin permeation of fibre reinforcements after shear deformation. Polym Compos 1997;18:6428.

[6] Smith P, Rudd CD, Long AC. The effect of shear deformation on the processing and mechanical properties of aligned reinforcements. Compos Sci Technol 1997;57:32744.

[7] Slade J, Sozer EM, Advani SG. Fluid impregnation of deformed preforms. J Reinf Plast Compos 2000;19:55268.

[8] Heardman E, Lekakou C, Bader MG. In-plane permeability of sheared fabrics. Compos Part A 2001;32:93340.

[9] Loix F, Badel P, Orgéas L, Geindreau C, Boisse P. Woven fabric permeability: from textile deformation to fluid flow mesoscale simulations. Compos Sci Technol 2008;68:1624–30.

[10] Bruschke MV, Advani SG. Flow of generalized newtonian fluids across a periodic array of cylinders. J Rheol 1993;37:47998.

[11] Velten K, Lutz A, Friedrich K. Quantitative characterization of porous materials in polymer processing. Compos Sci Technol 1999;59:495–504.

[12] Saunders RA, Lekakou C, Bader MG. Compression in the processing of polymer composites 2. Modelling of the viscoelastic compression of resin-impregnated fibre networks. Compos Sci Technol 1999;59:1483–94.

[13] Woods JK, Spelt PDM, Lee PD, Selerland T, Lawrence CJ. Creeping flows of power-law fluids through periodic arrays of elliptical cylinders. J Non-Newtonian Fluid Mech 2003;111:21128.

[14] Idris Z, Orgéas L, Geindreau C, Bloch J-F, Auriault J-L. Microsctructural effects on the flow law of power-law fluids through fibrous media. Modell Simul Mater Sci Eng 2004;12:995–1015.

[15] Orgéas L, Idris Z, Geindreau C, Bloch J-F, Auriault J-L. Modelling the flow of power-law fluids through anisotropic porous media at low pore Reynolds number. Chem Eng Sci 2006;61:4490–502.

[16] Chhabra RP, Comiti J, Machac I. Flow of non-newtonian fluids in fixed and fluidised beds. Chem Eng Sci 2001;56:1–27.

[17] Chhabra RP. Bubbles, drops, and particles in non-Newtonian fluids. Boca Raton (FL): CRC Press; 1993, ISBN 0 8493 6718 2 [Reprinted 1994. Second edition, 2006. CRC Press, Boca Raton].

[18] Orgéas L, Geindreau C, Auriault J-L, Bloch J-F. Upscaling the flow of generalised Newtonian fluids through anisotropic porous media. J Non-Newtonian Fluid Mech 2007;145:15–29.

[19] Ene H, Sanchez-Palencia E. Equations et phénomènes de surface pour écoulement dans un modèle de milieu poreux. J Méc 1975;14:73–108.

[20] Shah CB, Yortsos Y. Aspect of flow of power-law fluids in porous media. AIChE J 1995;41:1099112.

[21] Auriault J-L, Royer P, Geindreau C. Filtration law for power law fluids in anisotropic medium. Int J Eng Sci 2002;40:1151–63.

[22] Sanchez-Palencia E. Non-homogeneous media and vibration theory. Lectures notes in physics, 127. Berlin: Springer-Verlag; 1998.

[23] Darcy H. Les Fontaines Publiques de la Ville de Dijon. Paris: Victor Valmont; 1856.

[24] Boehler J-P. A simple derivation of representations of non-polynomial constitutive equations in some cases of anisotropy. ZAMM 1979;59:135–40.

[25] Badel P, Vidal-Salle E, Maire E, Boisse P. Simulation and tomography analysis of textile composite reinforcement deformation at the mesoscopic scale. Compos Sci Technol 2008;68:2433–40.